3-28-2019

Pace and Process of Active Folding and Fluvial Incision Across the Kantishna Hills Anticline, Central Alaska

A. M. Bender
United States Geological Survey

R. O. Lease
United States Geological Survey

P. J. Haeussler
United States Geological Survey

T. Rittenour
Utah State University

L. B. Corbett
University of Vermont

See next page for additional authors

Recommended Citation

Bender, A. M., Lease, R. O., Haeussler, P. J., Rittenour, T., Corbett, L. B., Bierman, P. R., & Caffee, M. W. (2019). Pace and process of active folding and fluvial incision across the Kantishna Hills anticline, central Alaska. Geophysical Research Letters, 46, 3235– 3244. https://doi.org/10.1029/2018GL081509

Authors

A. M. Bender, R. O. Lease, P. J. Haeussler, T. Rittenour, L. B. Corbett, P. R. Bierman, and M. W. Caffee

Geophysical Research Letters

RESEARCH LETTER

Correspondence to:
A. M. Bender,
abender@usgs.gov

Pace and Process of Active Folding and Fluvial Incision Across the Kantishna Hills Anticline, Central Alaska

A. M. Bender[1] [iD], **R. O. Lease[1]** [iD], **P. J. Haeussler[1]** [iD], **T. Rittenour[2]**, **L. B. Corbett[3]** [iD], **P. R. Bierman[3]** [iD], and **M. W. Caffee[4]** [iD]
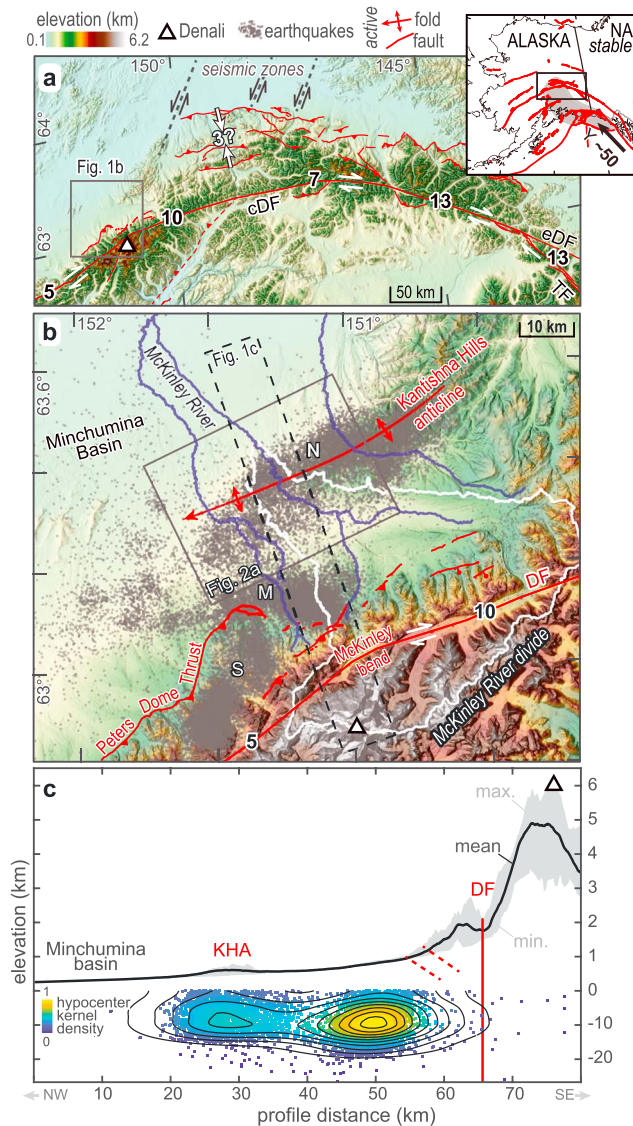
[1]U.S. Geological Survey, Anchorage, Alaska, USA, [2]Department of Geology, Utah State University, Logan, Utah, USA, [3]Department of Geology, University of Vermont, Burlington, Vermont, USA, [4]Department of Physics and Astronomy and Department of Earth, Purdue University, West Lafayette, Indiana, USA

Abstract Rates of northern Alaska Range thrust system deformation are poorly constrained. Shortening at the system's west end is focused on the Kantishna Hills anticline. Where the McKinley River cuts across the anticline, the landscape records both Late Pleistocene deformation and climatic change. New optically stimulated luminescence and cosmogenic [10]Be depth profile dates of three McKinley River terrace levels (~22, ~18, and ~14–9 ka) match independently determined ages of local glacial maxima, consistent with climate-driven terrace formation. Terrace ages quantify rates of differential bedrock incision, uplift, and shortening based on fault depth inferred from microseismicity. Differential rock uplift and incision (≤1.4 m/kyr) drive significant channel width narrowing in response to ongoing folding at a shortening rate of ~1.2 m/kyr. Our results constrain northern Alaska Range thrust system deformation rates, and elucidate superimposed landscape responses to Late Pleistocene climate change and active folding with broad geomorphic implications.

Plain Language Summary Where plate tectonics deforms Earth's surface, river landscapes hold information about the distribution and rate of earthquake-related deformation over thousands of years. The processes that form these landscapes remain uncertain. Here we study the landscape where the McKinley River cuts across the Kantishna Hills anticline to quantify previously unknown rates of earthquake-related tectonic deformation in intracontinental Alaska, and investigate the mechanisms by which this landscape evolved. We date McKinley River terraces that were the river channel ~22, ~18, and ~14–9 ka; the ages match independent ages of regional glacial advances and hence indicate climatic control on river terrace formation. Digital topography analysis shows that the terraces have been folded and uplifted above the channel at rates up to ~1.4 m/kyr associated with shortening at ~1.2 m/kyr. The McKinley River channel narrows and slightly steepens across the fold where uplift rates are highest, indicating that the river adjusts to uplift primarily by reducing channel width and not by steepening as common incision models assume. Kantishna Hills anticline shortening accounts for ~10% of the total ~13-mm/year plate strain rate; ~6 mm/year remains unaccounted for at this latitude and is likely distributed across structures south of the Denali Fault.

1. Introduction

Erosion and tectonic deformation compete to drive the evolution of mountainous landscapes that, in turn, hold information about the rates and mechanisms of these processes (e.g., Whipple et al., 2013). Bedrock river incision sets the lower elevation boundary over most of Earth's unglaciated surface (e.g., Kirby & Whipple, 2012), and fault-related folding represents a primary means by which tectonic deformation elevates upper crustal rock and the overlying landscape (e.g., Hubert-Ferrari et al., 2007). Consequently, studies of differential bedrock incision and uplift of river channels and landforms (i.e., strath terraces; Schanz et al., 2018) underpin much of our understanding of the rate and distribution of continental tectonic deformation at intermediate ($\leq 10^6$ year) time scales (e.g., Burbank et al., 1996; Hubert-Ferrari et al., 2007; Lavé & Avouac, 2000). Importantly, comparison of such fluvial geomorphic records with decadal rates and patterns of lithospheric deformation inferred from geodesy may reveal geologic strain rate deficits or surpluses indicative of concealed earthquake hazard (e.g., Kirby et al., 2008).

AGU
100
ADVANCING EARTH
AND SPACE SCIENCE

Geophysical Research Letters

10.1029/2018GL081509

Figure 1. Kantishna Hills anticline setting. Inset locates Figure 1a and shows the Yakutat microplate (Y; gray shaded area) and convergence on North America (NA; ~50 mm/year NNW; Elliott et al., 2010). (a) Neotectonic setting. Black numbers are slip rates (m/kyr) from Haeussler et al. (2017a) for the combined Totschunda Fault (TF) and eastern Denali Faults (eDF), and segments of the central Denali Fault (cDF). Queried 3-m/kyr shortening rate from Bemis et al. (2015). Seismic zones from Tape et al. (2015). (b) Geomorphic and seismotectonic setting. Peters Dome thrust from Bemis et al. (2012) and other thrust and normal faults from Burkett et al. (2016). Northern (N), middle (M), and southern (S) Kantishna seismic cluster (Ruppert et al., 2008). (c) Swath profiles (10 km wide) of topography, schematic faults, and earthquake hypocenters. Hypocenters colored by 250-m bandwidth kernel density, contours show density changes on 10% intervals.

Despite the utility of fluvial archives of active tectonic deformation, debate continues over the fundamental processes behind these geomorphic records. For example, river profile analysis holds promise for the estimation of rock uplift rates directly from digital topography (e.g., Goren et al., 2014), but most extant approaches utilize a stream power incision model that neglects the possibly significant roles of dynamic channel width adjustment and sediment flux (Yanites, 2018, and references therein). Moreover, while researchers commonly infer uplift rates from the incision of dated fluvial strath terraces, mechanisms of terrace formation may vary (e.g., climatic forcing versus autogenic effects; Schanz et al., 2018) with key implications for interpreting tectonic rates (e.g., Finnegan et al., 2014). Hence, advancing our ability to interpret the signature of active tectonics and related hazards from fluvial geomorphic records requires input from field studies that quantify both the pace and process of landscape response.

Here we exploit a well-preserved geomorphic record of Late Pleistocene climate variability, active folding, and bedrock incision where the McKinley River cuts across the Kantishna Hills anticline in central Alaska. We use digital topography and field measurements to characterize the magnitude of folding of three McKinley River strath terrace levels. We constrain terrace ages using optically stimulated luminescence (OSL) and cosmogenic ^{10}Be samples of abandoned channel deposits. Analysis of Kantishna seismic cluster hypocenter distribution beneath the fold delimits the depth to a probable structural detachment. We examine McKinley River channel geometries across the fold to ascertain how the river channel presently responds to ongoing differential rock uplift. Our results place the first direct quantitative bounds on Late Pleistocene rates of deformation in the northern Alaska Range thrust system, exemplify climatic modulation of river terrace formation, and demonstrate a case where dynamic channel width plays a critical role in bedrock river incision response to differential uplift.

2. Background and Field Area

Intracontinental Alaska deforms in response to the north-northwest directed collision and flat-slab subduction of the Yakutat microplate (Elliott et al., 2013). Shortening at the southern Alaska margin takes up ~75% of the geodetically inferred ~50-mm/year Yakutat convergence velocity (Elliott et al., 2013). The southern Alaska lithospheric block transmits the remaining ~25% several hundred kilometers inland to the Denali Fault, where Late Pleistocene average rates of ~13-m/kyr dextral slip account for the residual plate velocity near the Totschunda Fault junction, but decrease westward to ~5 m/kyr over ~350 km along strike (Haeussler et al., 2017; Matmon et al., 2006; Mériaux et al., 2009; Figure 1a).

Researchers attribute the westward decrease in slip rate to right trans-pression across thrust faults that splay southwest off the Denali Fault (Haeussler et al., 2017), and to partitioning of the north-northwest component of southern Alaska block convergence across an array of thrust faults and folds situated north of, and parallel to, the Denali Fault (the northern Alaska Range thrust system; Bemis & Wallace, 2007; Haeussler, 2008; Mériaux et al., 2009; Bemis et al., 2012, 2015; Haeussler, Matmon, et al., 2017). This deformation fits a kinematic model in which the southern Alaska block (a) rotates counterclockwise at rates equivalent to Denali Fault slip,

(b) shortens internally across the right-transpressive faults, (c) extrudes westward at a modest pace, and (d) translates north-northwest and indents central Alaska at a rate commensurate with shortening across the northern Alaska Range thrust system (Haeussler, Matmon, et al., 2017). Absent direct constraints, Late Pleistocene rates of southern and central Alaska deformation off the Denali Fault remain unquantified, leaving unclear the far-field distribution of strain related to the Yakutat microplate collision (e.g., Bemis et al., 2015; Haeussler, Matmon, et al., 2017).

We focus on the Kantishna Hills anticline, the primary structure at the west end of the northern Alaska Range thrust system (Figure 1a). Basin analysis implies thrust system initiation in Oligocene-Miocene time (Ridgway et al., 2007), broadly concurrent with the onset of Yakutat microplate collision (Lease et al., 2016, and references therein). Subsequently, structural and stratigraphic data indicate progressive northward advance and lateral propagation of northern Alaska Range thrust system structures above a gently south dipping basal detachment (Bemis & Wallace, 2007; Ridgway et al., 2007). Deformed river terraces and offset postglacial surfaces of unknown age provide evidence for ongoing deformation through Quaternary time with inferred rates of shortening approaching 3 m/kyr (Bemis et al., 2015). Assuming 13 mm/year of far-field Yakutat convergence (Elliott et al., 2013; Haeussler, Matmon, et al., 2017), such shortening is consistent with the average 7–10-m/kyr Denali Fault slip rates south of the thrust system (Haeussler, Saltus, et al., 2017). Given unconstrained rates of transpression south of the Denali Fault, however, the rate of northern Alaska Range shortening may be much lower, and remains untested by direct dating of deformed geomorphic markers.

We conduct such a test using the seismically active Kantishna Hills anticline (Lesh & Ridgway, 2007; Figure 1b). The anticline projects the west-southwest strike of the thrust system into the Minchumina basin, ~40 km north of the McKinley restraining bend of the Denali Fault (Burkett et al., 2016; Haeussler, 2008). Active structures between the Kantishna Hills anticline and the Denali Fault comprise down-to-the-south normal fault scarps associated with the McKinley bend, and discontinuous ≤1-km-long thrust scarps that record up to two late Holocene earthquakes (Burkett et al., 2016). In contrast, structural continuity and prominence of the Kantishna Hills anticline indicate that it is the primary structure absorbing north-northwest directed shortening at the west end of the thrust system.

The Kantishna Hills anticline provides a textbook geomorphic example of active folding. Several trunk rivers that drain the north flank of the rapidly rising Denali massif (exhumation >1 km/Myr since ~6 Ma; Fitzgerald et al., 1993) flow west-southwest around the fold, in the direction of apparent plunge, before incising across the trend of the structure (cf., Keller & DeVecchio, 2013; Figure 1b). Where the McKinley River cuts one of these water gaps (termed Eagle Gorge), Lesh and Ridgway (2007) observed the channel planform change from wide, alluvial, and braided both upstream and downstream to a single mixed bedrock-alluvial thread entrenched across the fold into Paleozoic schist (Reed, 1961). Lesh and Ridgway (2007) interpreted this planform change, along with Hack gradient index variations (see Kirby & Whipple, 2012) and the presence of deeply incised McKinley River strath terraces along Eagle Gorge to collectively represent ongoing differential uplift and incision of the Kantishna Hills anticline. This interpretation assumes that strath terraces serve as passive markers of fold growth relative to the McKinley River channel (e.g., Hubert-Ferrari et al., 2007); hence, dating these features would quantify deformation rates associated with terrace incision (e.g., Burbank et al., 1996; Lavé & Avouac, 2000).

A persistent cluster of small earthquakes (the northern Kantishna seismic cluster; Ruppert et al., 2008) occurs beneath the Kantishna Hills anticline, providing further evidence for active deformation (Ruppert et al., 2008; Figures 1b and 1c). These earthquakes, typically $M \leq 3$ and detected at near-steady rates since initial seismic network establishment in 1968, compose the northernmost subgroup of three Kantishna seismic clusters between the anticline and the Denali Fault (Ruppert et al., 2008). Most (~90%) of these earthquakes occur within the uppermost 12 km (Ruppert et al., 2008) of the locally 30–35-km-thick crust (e.g., Miller et al., 2018). Focal mechanisms within the northern Kantishna cluster indicate primarily strike-slip and thrust fault earthquakes, with P axes oriented north-northwest in agreement with the west-southwest trend of the overlying fold (Ruppert et al., 2008). Spatial overlap and mutually consistent stress orientations intimate a yet-untested linkage between active folding of the Kantishna Hills anticline and the underlying seismicity (Bemis et al., 2012; Ruppert et al., 2008).
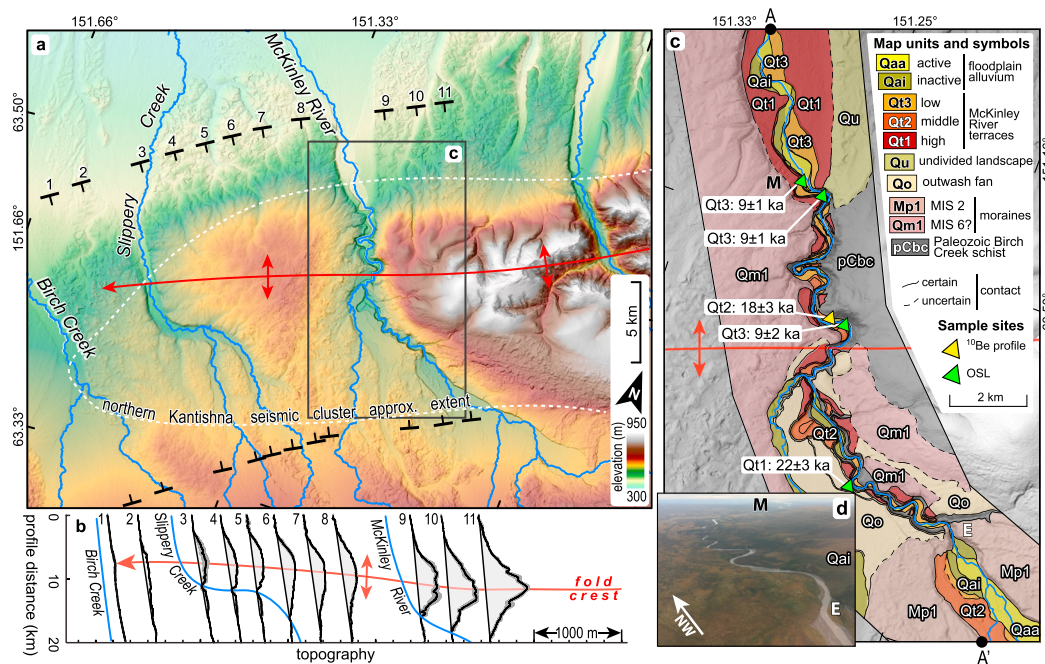
Figure 2. Geomorphic expression of the Kantishna Hills anticline. (a) IfSAR-derived hillshade, elevation, and trunk river network. Black numbers and *T* symbols indicate 1-km-wide swath profiles of topography depicted in Figure 1b. (b) Swath profiles (1 km wide) of topography across the Kantishna Hills fold crest, with trunk rivers schematically depicted. (c) Surficial geologic map of Eagle Gorge. Black dots A and A′ indicate start and end of Figure 3 profiles. (d) Aerial photo of Eagle Gorge looking north-northwest from the Gorge entrance (E) toward the mouth (M) also shown on Figure 2c.

3. Methods and Results

3.1. Surface Deformation From Field Mapping and Digital Topography Analysis

We characterized surface deformation across the Kantishna Hills anticline using field-based validation of remote, reconnaissance-level digital mapping and topography analysis. We used 5-m/pixel aerial interferometric synthetic aperture radar-based digital topography (IfSAR DEM; https://lta.cr.usgs.gov/IFSAR_Alaska) to characterize surface folding at the regional scale (i.e., ~30 by 20 km; Figure 2a) and to map geomorphology, including three levels of McKinley River strath terraces, at the 1:10,000 scale. In the field, we excavated, measured, and described the three strath terrace levels (which we term Qt1–3) and associated alluvial cover deposits at multiple locations across the Kantishna Hills anticline along Eagle Gorge (Figures 2a–2d). We refined the remote mapping based on field observations, and used the IfSAR DEM to quantify terrace deformation along profiles across the fold. We constructed terrace profiles by extracting pixel elevations from the IfSAR DEM within mapped terrace treads where slope ≤ 5°, and averaging the resulting elevation "cloud" on 250-m profile distance bins (Figure 3a). Subtracting both the IfSAR-derived modern channel level and field-measured channel deposit thickness (Qt1 ~12 m, Qt2 ~9 m, Qt3 ~6 m) from the tread elevations yields profiles of strath height that quantify differential bedrock incision across the fold along the McKinley River (Figure 3b).

Kilometer-wide swath profiles of IfSAR-derived elevation reveal a single southwest trending anticlinal fold that projects along the strike of the contiguous mapped bedrock Kantishna Hills anticline (Reed, 1961; Figures 2a and 2b). This broad surface fold retains a constant ~15-km half-wavelength and decreases monotonically in amplitude along-trend from a maximum of ~200 m near Eagle Gorge to the regional base level set by the Minchumina basin east of Birch Creek, ~20 km to the southwest. The surface fold warps glacial landforms with inferred ages exceeding 191 ka (i.e., >MIS 6; Burkett et al., 2016), and closely matches the map distribution of earthquakes within the northern Kantishna cluster. The degree of erosional dissection of the fold appears to decrease in the direction of plunge, and several trunk rivers draining the northern Alaska Range flow southwest along the south flank of the Kantishna Hills anticline before cutting across it. These observations are collectively consistent with expectations of landscape response to active, southwest propagating fold growth (e.g., Keller & DeVecchio, 2013).
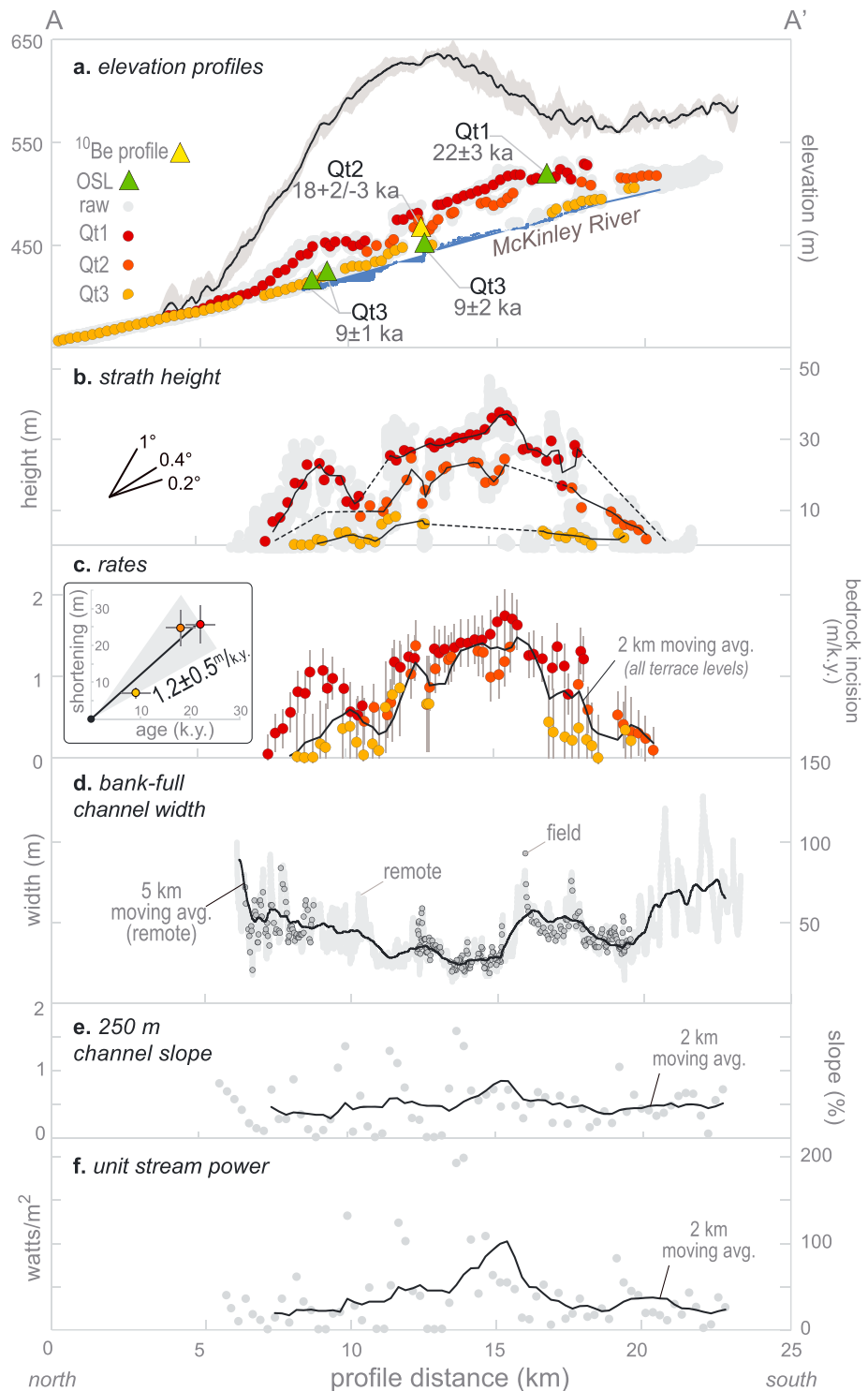
Figure 3. Profiles across the Kantishna Hills anticline, projected onto profile A-A′, indicated on Figure 2c. (a) Terrace tread pixel elevations where slope ≤ 5° (gray dots) averaged on 250-m distance bins (colored dots), McKinley River channel, age sample sites, and swath profile 8 (located on Figure 2a). (b) Strath heights. (c) Rates; inset plots terrace age against shortening to compute the time-averaged shortening rate, profile plots bedrock incision rate, which we equate with the rock uplift rate, across the fold. (d) Bankfull channel width measured in the field (dark gray dots) and remotely (light gray dots). Black line is 5-km moving average of remote width measurements. (e) IfSAR-derived channel slope on 250-m reach midpoints (gray dots) and smoothed on a 2-km moving average (black line). (f) Unit stream power on 250-m reach midpoints (gray dots) and smoothed on a 2-km moving average (black line).

Where the McKinley River crosses the anticline through Eagle Gorge, terrace tread elevations and strath heights vary systematically with adjacent surface folding, despite some scatter and downstream discontinuity (Figures 3a and 3b). Strath heights near the canyon entrance and outlet approach river level, but achieve local maxima within the fold crest (Qt1 ~37 m, Qt2 ~25 m, Qt3 ~8 m). McKinley River treads and straths tilt (a) to the north within the north flank of the fold (Qt1 ~1°, Qt3 ~0.2°), (b) to the north across the fold crest (Qt1–3 ~0.1°), and (c) to the southeast within the south flank of the fold (Qt2 ~0.4°, Qt3 ~0.2°). Agreement between strath heights and the elevation of the surface fold into which the terraces are cut indicates that folding, following terrace abandonment, regulates the observed tread and strath geometry. Dates of terrace abandonment thus constrain rates of active folding.

3.2. McKinley River Terrace Chronology

Five OSL samples and a cosmogenic ^{10}Be depth profile allow us to date relict McKinley River deposits on three terrace levels across the Kantishna Hills anticline (Tables S1–S6 and Figures S1–S7). To constrain terrace abandonment timing, we collected OSL samples of silt and fine sand near the stratigraphic top of fluvial deposits on the highest (Qt1, $n = 1$) and lowest (Qt3, $n = 4$) strath terraces (Figures 2c and S2–S5) using opaque metal pipes (Nelson et al., 2015). We analyzed quartz grains from these samples at the Utah State University Luminescence Laboratory following standard single-aliquot regenerative-dose procedures (Murray & Wintle, 2000, 2003; Wintle & Murray, 2006). See supporting information for further details on OSL dating methods, result, and age determination (Aitken & Alldred, 1972; Gibson, 2009; Guérin et al., 2011; Galbraith & Roberts, 2012; Prescott & Hutton, 1994). Lacking sand lenses for OSL dating of the middle terrace level (Qt2), we sampled the 250–1,000-μm sand fraction of terrace gravel from five ~10-cm-thick stratigraphic horizons at 30-cm vertical intervals to measure in situ ^{10}Be concentrations (Figures 2c and S6). We prepared these samples at the University of Vermont (Corbett et al., 2016), measured ^{10}Be/^{9}Be ratios at the Purdue Rare Isotope Measurement Laboratory, and used the MATLAB-based calculator of Hidy et al. (2010) to model an abandonment age from the ^{10}Be concentration-depth profile (Figures S6 and S7; (Nishiizumi et al., 2007).

The McKinley River strath terrace samples yield stratigraphically and geomorphically consistent ages (Figures 2c, 3a, and S1–S7 and Tables S1–S6). Sandy sediment near the top of terrace stratigraphy at three locations on Qt3 all yield OSL ages of 9 ka with 1–2-ka uncertainties (1σ, as with all uncertainties quoted in this paper), and cap a deeper sand-over-gravel horizon with an OSL age of 14 ± 2 ka at one site. The ^{10}Be depth-concentration profile in the upper third of the ~9-m-thick gravel on Qt2 provides an age of 18 ± 3 ka. A single sand horizon near the top of the ~12-m-thick gravel of Qt1 yields an OSL age of 22 ± 3 ka. Within uncertainty, all terrace ages except the youngest (which we replicate at three locations) broadly agree with cosmogenic (Dortch et al., 2010) and calibrated radiocarbon ages (Briner et al., 2017) of upstream moraines that mark glacial maxima at 20.8–22.3, 16.7–17.6, and 14.0–15.1 ka. This agreement suggests climatic modulation of terrace formation (e.g., Pan et al., 2003) and supports our assumption of terrace isochrony along the ~15-km length of Eagle Gorge.

3.3. Rates of Bedrock Incision, Rock Uplift, and Shortening

We equate differential bedrock incision along the McKinley River with rock uplift across the Kantishna Hills anticline, and compute these rates as the quotient of strath height and terrace age. This simple estimation of rock uplift relies on several assumptions, supported by key field and DEM observations, which we detail in the supporting information. Rates of rock uplift and incision computed on each terrace level (a) overlap along the profile within uncertainty, indicating rate steadiness over time, and (b) vary systematically with the surface fold elevations adjacent to Eagle Gorge, suggesting that folding controls the pattern of terrace incision (Figure 3c). Vertical rates near the canyon entrance and outlet approach zero for each level and are highest at the fold crest (Qt1, 1.8 ± 0.3 m/kyr; Qt2, 1.4 ± 0.3 m/kyr; Qt3, 0.9 ± 0.7 m/kyr), averaging ~1.4 m/kyr within a 2-km moving window.

Assuming that folding governs the observed strath height profiles, numerical integration of these profiles yields the area of rock uplifted beneath each strath (Figures 3b and S8 and Table S7), which in turn enables computation of shortening, provided that there are constraints on the depth of related faulting (e.g., Hubert-Ferrari et al., 2007; Lavé & Avouac, 2000). We infer the presence of, and delimit the depth to, a subhorizontal detachment fault beneath the terraces based on 7,710 small ($M_L < 3$) earthquake hypocenters recorded in the Kantishna seismic cluster between 1988 and 2018 (Ruppert et al., 2008; earthquake.alaska.edu). We compute

maximum hypocenter density at 10-km depth along an 80×10-km swath profile centered over Eagle Gorge (Figure 1b), so we infer the depth to detachment at 10 km and assign a nominal uncertainty of 2 km based on the density contours (Figures 1c and S8; cf. Carena et al., 2002). See supporting information for additional details on earthquake hypocenter data and density calculation. The slope of a line fit through the origin (i.e., the modern strath) to computed shortening and terrace age yields the time-averaged rate of shortening recorded by the folded terraces (Figure 3c). Uplifted rock area beneath each strath (Qt1 ~0.26 km², Qt2 ~0.25 km², Qt3 ~0.07 km²; uncertainties on the order of 1–4%) implies time-averaged shortening at a rate of 1.2 ± 0.5 m/kyr since 22 ± 3 ka.

3.4. Unit Stream Power Adjustment to Active Folding

We quantify the contemporary McKinley River channel response to growth of the Kantishna Hills anticline by computing unit stream power at 250-m distance intervals across the fold through Eagle Gorge. Unit stream power represents the energy that a volume of water dissipates into a river channel's bed and banks per unit channel width at a rate governed by channel slope, and is proportional to incision rate (e.g., Whipple et al., 2013). This relationship implies that adjustments to both channel slope and width modulate fluvial capacity to incise across spatial gradients in rock uplift, contrasting with slope-dependent incision models (cf., Kirby & Whipple, 2012) but consistent with field observations from a range of tectonic settings (e.g., Allen et al., 2013; Amos & Burbank, 2007; Duvall et al., 2004; Yanites et al., 2010). We compute unit stream power at 250-m intervals (Text S2) based on IfSAR-derived channel slope, field and remotely measured channel width (Fisher et al., 2013), and discharge (Curran et al., 2016).

Field and remote measurements of bankfull channel width closely agree through Eagle Gorge (Figures 3d, S9a, and S9b). Remotely measured channel width at the Gorge entrance and outlet locally approach 140 m, while minimum values of 13 m (remote) and 19 m (field) occur where the McKinley River crosses the fold crest. Moving average (5 river km) remotely measured channel width decreases from ~77 m (entrance) to ~24 m in the fold crest. These estimates suggest an average threefold (but up to approximately tenfold) channel width reduction across the anticline crest. Where the width is narrowest, exposed angular blocks and fluted straths in the mixed alluvial-bedrock channel imply erosion by both plucking and abrasion (Figure S9c; Whipple et al., 2013) in the absence of erodibility-enhancing rock type changes (e.g., Duvall et al., 2004). IfSAR-derived channel slope remains low through Eagle Gorge (Figure 3e) but increases to ~1% across the fold crest, coincident with the location of the narrowest channel widths. Combined with 20% exceedance probability discharge (Curran et al., 2016), estimates of channel slope and bankfull width predict an average fivefold increase in McKinley River unit stream power, from ~25 W/m² near the Gorge entrance and outlet to ~130 W/m² across the anticline crest (Figure 3e).

4. Discussion and Implications

Our results constrain the regional distribution and kinematics of surface folding across the Kantishna Hills anticline, demonstrate the climatic origin of the McKinley River terraces, quantify deformation and incision rates through Eagle Gorge, and elucidate the ongoing channel response to active folding. At the regional scale, we observe an ~20-km-long surface fold that plunges ~200 m to the southwest, diverts three trunk rivers in the direction of plunge, and becomes increasingly dissected by erosion along strike opposite the direction of plunge (Figures 2a and 2b). Together, these observations strongly suggest that active folding of the Kantishna Hills anticline propagates to the southwest, consistent with geomorphic expectations of lateral fold growth (e.g., Keller & DeVecchio, 2013) and with the inference of Lesh and Ridgeway (2007). Whereas Lesh and Ridgeway (2007) suggested that Eagle Gorge approximately delimits the lateral extent of Kantishna Hills folding, our observations extend the distribution of surface deformation ~20 km to the southwest and are consistent with the areal extent of the seismic cluster.

The systematic downstream variation of McKinley River terrace tread elevations and strath heights, in concert with the adjacent surface fold, place kinematic constraints on the style of folding at Eagle Gorge. Where preserved, strath heights show near-symmetric increases in tilt between successively higher terraces within the north (forelimb) and south (backlimb) flanks of the fold (Figure 3b), indicative of growth by progressive limb rotation and broadly consistent with end-member models of either simple detachment or fault bend folding (e.g., Hubert-Ferrari et al., 2007; Lavé & Avouac, 2000). Such folds generally develop above stratigraphic contrasts in mechanical competence, where strong strata overlie a relatively weak horizon at depth

(i.e., the detachment). The Birch Creek schist coring the Kantishna Hills anticline contains horizons of varying competency (e.g., Reed, 1961) that may promote detachment in the presence of distributed plate boundary strain. For example, Bemis and Wallace (2007) show that a basal detachment fault developed in the Birch Creek schist, dipping ~2° south at depths of 7–9 km, best explains surface structural and stratigraphic data on a transect across the northern Alaska Range thrust system ~125 km east of the Kantishna Hills. We infer the presence of a similar detachment beneath the Kantishna Hills anticline, based on folded terrace geometries and underlying microseismicity focused at ~10-km depth.

We report new ages of the McKinley River terrace deposits (~22, ~18, and ~14–9 ka) that closely match the timing of local glacial maxima (e.g., Briner et al., 2017). This temporal agreement implies that climatic conditions favorable to glacial advances also perturbed the McKinley River discharge to sediment load ratio, forcing aggradation of the 6–12-m-thick channel deposits that now cap the terraces superimposed on the growing fold (cf., Pan et al., 2003). The duration of incisional hiatuses implicit in the thick terrace deposits appear negligible relative to the ~22-kyr measurement interval, given the apparent temporal steadiness of bedrock incision rates across the fold (Figure 3c; Finnegan et al., 2014; Gallen et al., 2015). In contrast with climatically modulated intervals of terrace-forming aggradation that briefly impede bedrock incision, several lines of evidence suggest that sediment flux may regulate long-term bedrock incision of the Kantishna Hills anticline.

We weigh key field observations against model-derived insights on sediment flux-dependent bedrock incision (e.g., Whipple & Tucker, 2002; Yanites, 2018). First, the highest bedrock incision rates (~1.4 m/kyr since ~22 ka) occur across the fold crest, where channel narrowing (approximately threefold) and steepening (<twofold) enhance transport and erosive capacity by producing an approximately fivefold increase in unit stream power (Figures 3a–3e). Second, the McKinley River drains the rapidly exhuming Denali massif (>1 km/Myr since ~6 Ma; Fitzgerald et al., 1993), implying a high background rate of catchment sediment production and ample tool supply (e.g., Whipple & Tucker, 2002). The rapid sediment production yields broad alluvial channel reaches upstream and downstream of Eagle Gorge (Figures 2c and 2d). Within the gorge across the fold, however, the alluvial cover is thin and discontinuous; extensive bedrock exposure along the channel banks provides conditions favorable for bedrock incision (Figure S1c; e.g., Whipple & Tucker, 2002; Yanites, 2018). Taken together, the observed adjustments to channel width, slope, transport capacity, and sediment cover across the fold closely match patterns of channel response to changes in rock uplift predicted by models that allow these factors to co-evolve (Yanites, 2018). We suggest that McKinley River incision, governed by tectonically modulated sediment flux, keeps pace with rock uplift across the Kantishna Hills anticline primarily by narrowing its channel width, rather than by channel steepening as Lesh and Ridgeway (2007) suggested. If true, this represents a case in which channel width narrowing sustains the fluvial response to differential uplift over time, unlike the more commonly recognized transient width response (e.g., Amos & Burbank, 2007) that ultimately yields to channel steepening that is ubiquitously encoded in conventional incision models (e.g., Kirby & Whipple, 2012). Our results contribute to a growing body of field (e.g., Allen et al., 2013; Lavé & Avouac, 2000; Yanites et al., 2010) and model-based (e.g., Yanites, 2018) evidence that emphasize the significance of channel width adjustment to differential rock uplift on Late Quaternary time scales.

Ages of the climatic terraces superimposed on the growing Kantishna Hills anticline quantify shortening at a rate of 1.2 ± 0.5 m/kyr since 22 ± 3 ka across the fold. This rate, which depends in part on depth-to-detachment but not on fault geometry, provides the first direct rate constraint on total Late Pleistocene shortening across the Northern Alaska Range thrust system, and falls within the range of rates inferred across the system ~125 km to the east (1–3 m/kyr; Bemis et al., 2015). The Kantishna Hills anticline localizes deformation at the west end of the northern Alaska Range thrust system; hence, if shortening across the northern Alaska Range thrust system accommodates northwest translation of southern Alaska lithosphere via indentation at an equivalent rate (e.g., Bemis et al., 2015; Haeussler, Matmon, et al., 2017), our estimated rate of shortening across the Kantishna Hills constrains the speed of southern Alaska translation to ~1.2 m/kyr since ~22 ka.

5. Conclusions

New ages of strath terraces that flank the McKinley River across the Kantishna Hills anticline place quantitative bounds on rates of shortening (~1.2 m/kyr) and differential rock uplift and incision (≤1.4 m/kyr) since ~22 ka. Close agreement between the new terrace ages and dates of regional glacial maxima (e.g., Briner

et al., 2017) imply a climatic origin for the McKinley River terraces. Across the anticline crest, where rock uplift rates approach local maxima, an approximately threefold reduction in McKinley River channel width implies an average fivefold increase in unit stream power with minimal concomitant increases in slope. This spatiotemporally sustained channel width adjustment to fold-driven rock uplift likely reflects the dependence of bedrock incision on sediment flux governed by climatic (i.e., glacial advance or retreat) and tectonic (i.e., exhumation rates >1 km/Myr; Fitzgerald et al., 1993) conditions in the catchment upstream that impede or enhance downcutting, and challenges the ubiquitous applicability of slope-dependent incision models. Our results provide the first direct constraint on rates of Late Pleistocene deformation in the Northern Alaska Range thrust system. Shortening across the Kantishna Hills anticline, the primary structure at the west end of the thrust system, occurs at a rate consistent with geomorphically inferred but chronologically unconstrained shortening rates across a much broader part of the system ~125 km to the east (1–3 m/kyr; Bemis et al., 2015), implying a minimum speed limit for the north-northwest translation of the southern Alaska block of 1.2 ± 0.5 m/kyr. This rate represents ~10% of the residual Yakutat velocity that propagated onto the Denali Fault system in interior Alaska. Up to ~6 m/kyr of horizontal geodetic velocity remains unaccounted for but is likely distributed across right-transpressive faults south of the Denali Fault.

References

Aitken, M. J., & Alldred, J. C. (1972). The assessment of error limits in thermoluminescence dating. *Archaeometry*, *14*(2), 257–267. https://doi.org/10.1111/j.1475-4754.1972.tb00068.x

Allen, G. H., Barnes, J. B., Pavelsky, T. M., & Kirby, E. (2013). Lithologic and tectonic controls on bedrock channel form at the northwest Himalayan front. *Journal of Geophysical Research: Earth Surface*, *118*, 1806–1825. https://doi.org/10.1002/jgrf.20113

Amos, C. B., & Burbank, D. W. (2007). Channel width response to differential uplift. *Journal of Geophysical Research*, *112*, F02010. https://doi.org/10.1029/2006JF000672

Bemis, S. P., Carver, G. A., & Koehler, R. D. (2012). The Quaternary thrust system of the northern Alaska Range. *Geosphere*, *8*(1), 196–205. https://doi.org/10.1130/GES00695.1

Bemis, S. P., and W. K. Wallace (2007). Neotectonic framework of the north-central Alaska Range foothills. In K. D. Ridgway, J. M. Trop, J. M. G. Glen, & J. M. O'Neill (Eds.), *Tectonic Growth of a Collisional Continental Margin: Crustal Evolution of Southern Alaska*, *Geological Society of America Special Paper* (Vol. 431, pp. 549–572). Boulder, CO: Geological Society of America. https://doi.org/10.1130/2007.2431(21)

Bemis, S. P., Weldon, R. J., & Carver, G. A. (2015). Slip partitioning along a continuously curved fault: Quaternary geologic controls on Denali fault system slip partitioning, growth of the Alaska Range, and the tectonics of south-central Alaska. *Lithosphere*, *7*(3), 235–246. https://doi.org/10.1130/L352.1

Briner, J. P., Tulenko, J. P., Young, N. E., Baichtal, J. F., & Lesnek, A. (2017). The last deglaciation of Alaska. *Cuadernos de Investigación Geográfica*, *43*(2), 429–448. https://doi.org/10.18172/cig.3229

Burbank, D. W., Leland, J., Fielding, E., Anderson, R. S., Brozovic, N., Reid, M. R., & Duncan, C. (1996). Bedrock incision, rock uplift and threshold hillslopes in the northwestern Himalayas. *Nature*, *379*(6565), 505–510. https://doi.org/10.1038/379505a0

Burkett, C. A., Bemis, S. P., & Benowitz, J. A. (2016). Along-fault migration of the Mount McKinley restraining bend of the Denali fault defined by late Quaternary fault patterns and seismicity, Denali National Park & Preserve, Alaska. *Tectonophysics*, *693*, 489–506. https://doi.org/10.1016/j.tecto.2016.05.009

Carena, S., Suppe, J., & Kao, H. (2002). Active detachment of Taiwan illuminated by small earthquakes and its control of first-order topography. *Geology*, *30*(10), 935–938. https://doi.org/10.1130/0091-7613(2002)030<0935:ADOTIB>2.0.CO;2

Corbett, L. B., Bierman, P. R., & Rood, D. H. (2016). An approach for optimizing in situ cosmogenic ^{10}Be sample preparation. *Quaternary Geochronology*, *33*, 24–34. https://doi.org/10.1016/j.quageo.2016.02.001

Curran, J. H., Barth, N. A., Veilleux, A. G. & Ourso, R. T. (2016). Estimating flood magnitude and frequency at gaged and ungaged sites on streams in Alaska and conterminous basins in Canada, based on data through water year 2012 (no. 2016-5024). U.S. Geological Survey Scientific Investigations Report 2016–5024. https://doi.org/10.3133/sir20165024

Dortch, J. M., Owen, L. A., Caffee, M. W., & Brease, P. (2010). Late Quaternary glaciation and equilibrium line altitude variations of the McKinley River region, central Alaska Range. *Boreas*, *39*(2), 233–246. https://doi.org/10.1111/j.1502-3885.2009.00121.x

Duvall, A., Kirby, E., & Burbank, D. (2004). Tectonic and lithologic controls on bedrock channel profiles and processes in coastal California. *Journal of Geophysical Research*, *109*, F03002. https://doi.org/10.1029/2003JF000086

Elliott, J., Freymueller, J. T., & Larsen, C. F. (2013). Active tectonics of the St. Elias orogen, Alaska, observed with GPS measurements. *Journal of Geophysical Research: Solid Earth*, *118*, 5625–5642. https://doi.org/10.1002/jgrb.50341

Finnegan, N. J., Schumer, R., & Finnegan, S. (2014). A signature of transience in bedrock river incision rates over timescales of 10^4–10^7 years. *Nature*, *505*(7483), 391. https://doi.org/10.1038/nature12913

Fisher, G. B., Bookhagen, B., & Amos, C. B. (2013). Channel planform geometry and slopes from freely available high-spatial resolution imagery and DEM fusion: Implications for channel width scalings, erosion proxies, and fluvial signatures in tectonically active landscapes. *Geomorphology*, *194*, 46–56. https://doi.org/10.1016/j.geomorph.2013.04.011

Fitzgerald, P. G., Stump, E., & Redfield, T. F. (1993). Late Cenozoic uplift of Denali and its relation to relative plate motion and fault morphology. *Science*, *259*(5094), 497–499. https://doi.org/10.1126/science.259.5094.497

Galbraith, R. F., & Roberts, R. G. (2012). Statistical aspects of equivalent dose and error calculation and display in OSL dating: An overview and some recommendations. *Quaternary Geochronology*, *11*, 1–27. https://doi.org/10.1016/j.quageo.2012.04.020

Gallen, S. F., Pazzaglia, F. J., Wegmann, K. W., Pederson, J. L., & Gardner, T. W. (2015). The dynamic reference frame of rivers and apparent transience in incision rates. *Geology*, *43*(7), 623–626. https://doi.org/10.1130/G36692.1

Gibson, W. (2009). Mean precipitation for Alaska 1971–2000: National Park Service. Alaska Regional Office GIS Team, GeospatialDataset-2170508.

Goren, L., Fox, M., & Willett, S. D. (2014). Tectonics from fluvial topography using formal linear inversion: Theory and applications to the Inyo Mountains, California. *Journal of Geophysical Research: Earth Surface*, *119*, 1651–1681. https://doi.org/10.1002/2014JF003079

Guérin, G., Mercier, N., & Adamiec, G. (2011). Dose-rate conversion factors: Update: Ancient TL. *29*, 5–8.

Haeussler, P. J. (2008). An overview of the neotectonics of interior Alaska: Far-field deformation from the Yakutat microplate collision. In J. T. Freymueller, P. J. Haeussler, R. L. Wesson, & G. Ekström (Eds.), *Active Tectonics and Seismic Potential of Alaska*. https://doi.org/10.1029/179GM05

Haeussler, P. J., Matmon, A., Schwartz, D. P., & Seitz, G. G. (2017). Neotectonics of interior Alaska and the late Quaternary slip rate along the Denali fault system. *Geosphere*, *13*(5), 1445–1463. https://doi.org/10.1130/GES01447.1

Haeussler, P. J., Saltus, R. W., Stanley, R. G., Ruppert, N., Lewis, K., Karl, S. M., & Bender, A. (2017). The Peters Hills basin, a Neogene wedge-top basin on the Broad Pass thrust fault, south-central Alaska. *Geosphere*, *13*(5), 1464–1488. https://doi.org/10.1130/GES01487.1

Hidy, A. J., Gosse, J. C., Pederson, J. L., Mattern, J. P., & Finkel, R. C. (2010). A geologically constrained Monte Carlo approach to modeling exposure ages from profiles of cosmogenic nuclides: An example from Lees Ferry, Arizona. *Geochemistry, Geophysics, Geosystems*, *11*, Q0AA10. https://doi.org/10.1029/2010GC003084

Hubert-Ferrari, A., Suppe, J., Gonzalez-Mieres, R., & Wang, X. (2007). Mechanisms of active folding of the landscape (southern Tian Shan, China). *Journal of Geophysical Research*, *112*, B03S09. https://doi.org/10.1029/2006JB004362

Keller, E. A., & DeVecchio, D. E. (2013). Tectonic geomorphology of active folding and development of transverse drainages. In J. Shroder & L. A. Owen (Eds.), *Treatise on Geomorphology, Tectonic Geomorphology* (Vol. 5, pp. 129–147). San Diego, CA: Academic Press. https://doi.org/10.1016/B978-0-12-374739-6.00088-9

Kirby, E., Whipple, K., & Harkins, N. (2008). Topography reveals seismic hazard. *Nature Geoscience*, *1*(8), 485–487. https://doi.org/10.1038/ngeo265

Kirby, E., & Whipple, K. X. (2012). Expression of active tectonics in erosional landscapes. *Journal of Structural Geology*, *44*, 54–75. https://doi.org/10.1016/j.jsg.2012.07.009

Lavé, J., & Avouac, J. P. (2000). Active folding of fluvial terraces across the Siwaliks Hills, Himalayas of central Nepal. *Journal of Geophysical Research*, *105*(B3), 5735–5770. https://doi.org/10.1029/1999JB900292

Lease, R. O., Haeussler, P. J., & O'Sullivan, P. (2016). Changing exhumation patterns during Cenozoic growth and glaciation of the Alaska Range: Insights from detrital thermochronology and geochronology. *Tectonics*, *35*, 934–955. https://doi.org/10.1002/2015TC004067

Lesh, M. E., & Ridgway, K. D. (2007). Geomorphic evidence of active transpressional deformation in the Tanana foreland basin, south-central Alaska. In K. D. Ridgway et al. (Eds.), *Tectonic Growth of a Collisional Continental Margin: Crustal Evolution of Southern Alaska, Geological Society of America Special Papers* (Vol. 431, pp. 573–592). Boulder, CO: GSA.

Matmon, A., Schwartz, D. P., Haeussler, P. J., Finkel, R., Lienkaemper, J. J., Stenner, H. D., & Dawson, T. E. (2006). Denali fault slip rates and Holocene–late Pleistocene kinematics of central Alaska. *Geology*, *34*(8), 645–648. https://doi.org/10.1130/G22361.1

Mériaux, A.-S., Sieh, K., Finkel, R. C., Rubin, C. M., Taylor, M. H., Meltzner, A. J., & Ryerson, F. J. (2009). Kinematic behavior of southern Alaska constrained by westward decreasing postglacial slip rates on the Denali Fault, Alaska. *Journal of Geophysical Research*, *114*, B03404. https://doi.org/10.1029/2007JB005053

Miller, M. S., O'Driscoll, L. J., Porritt, R. W., & Roeske, S. M. (2018). Multiscale crustal architecture of Alaska inferred from *P* receiver functions. *Lithosphere*, *10*(2), 267–278. https://doi.org/10.1130/L701.1

Murray, A. S., & Wintle, A. G. (2000). Luminescence dating of quartz using an improved single-aliquot regenerative-dose protocol. *Radiation Measurements*, *32*(1), 57–73. https://doi.org/10.1016/S1350-4487(99)00253-X

Murray, A. S., & Wintle, A. G. (2003). The single aliquot regenerative dose protocol: Potential for improvements in reliability. *Radiation Measurements*, *37*(4–5), 377–381. https://doi.org/10.1016/S1350-4487(03)00053-2

Nelson, M. S., Gray, H. J., Johnson, J. A., Rittenour, T. M., Feathers, J. K., & Mahan, S. A. (2015). User guide for luminescence sampling in archaeological and geological contexts. *Advances in Archaeological Practice*, *3*(02), 166–177. https://doi.org/10.7183/2326-3768.3.2.166

Nishiizumi, K., Imamura, M., Caffee, M. W., Southon, J. R., Finkel, R. C., & McAninch, J. (2007). Absolute calibration of ^{10}Be AMS standards. *Nuclear Instruments and Methods in Physics Research section B: Beam Interactions with Materials and Atoms*, *258*(2), 403–413. https://doi.org/10.1016/j.nimb.2007.01.297

Pan, B., Burbank, D., Wang, Y., Wu, G., Li, J., & Guan, Q. (2003). A 900 ky record of strath terrace formation during glacial-interglacial transitions in northwest China. *Geology*, *31*(11), 957–960. https://doi.org/10.1130/G19685.1

Prescott, J. R., & Hutton, J. T. (1994). Cosmic ray contributions to dose rates for luminescence and ESR dating. *Radiation Measurements*, *23*(2-3), 497–500. https://doi.org/10.1016/1350-4487(94)90086-8

Reed, J. C. (1961). *Geology of the Mt. McKinley Quadrangle, Bulletin 1108–A* (pp. 1–36). Alaska: U.S. Geological Survey.

Ridgway, K. D., Thoms, E. E., Layer, P. W., Lesh, M. E., White, J. M., & Smith, S. V. (2007). Neogene transpressional foreland basin development on the north side of the central Alaska Range, Usibelli Group and Nenana Gravel, Tanana basin. In K. D. Ridgway et al. (Eds.), *Tectonic Growth of a Collisional Continental Margin: Crustal Evolution of Southern Alaska, Geological Society of America Special Papers* (Vol. 431, pp. 507–547). Boulder, CO: GSA.

Ruppert, N. A., Ridgway, K. D., Freymueller, J. T., Cross, R. S., & Hansen, R. A. (2008). Active tectonics of interior Alaska: Seismicity, GPS geodesy, and local geomorphology. In J. T. Freymueller, P. J. Haeussler, R. L. Wesson, & G. Ekström (Eds.), *Active Tectonics and Seismic Potential of Alaska*. https://doi.org/10.1029/179GM06

Schanz, S. A., Montgomery, D. R., Collins, B. D., & Duvall, A. R. (2018). Multiple paths to straths: A review and reassessment of terrace genesis. *Geomorphology*, *312*, 12–23. https://doi.org/10.1016/j.geomorph.2018.03.028

Tape, C., Silwal, V., Ji, C., Keyson, L., West, M. E., & Ruppert, N. (2015). Transtensional tectonics of the Minto Flats fault zone and Nenana basin, central Alaska. *Bulletin of the Seismological Society of America*, *105*(4), 2081–2100. https://doi.org/10.1785/0120150055

Whipple, K. X., DiBiase, R. A., & Crosby, B. T. (2013). Bedrock rivers. In J. Shroder & E. Wohl (Eds.), *Treatise on Geomorphology, Fluvial Geomorphology* (Vol. 9, pp. 550–573). San Diego, CA: Academic Press. https://doi.org/10.1016/B978-0-12-374739-6.00254-2

Whipple, K. X., & Tucker, G. E. (2002). Implications of sediment-flux-dependent river incision models for landscape evolution. *Journal of Geophysical Research*, *107*(B2), ETG-3. https://doi.org/10.1029/2000JB000044

Wintle, A. G., & Murray, A. S. (2006). A review of quartz optically stimulated luminescence characteristics and their relevance n single-aliquot regeneration dating protocols. *Radiation Measurements*, *41*(4), 369–391. https://doi.org/10.1016/j.radmeas.2005.11.001

Yanites, B. J. (2018). The dynamics of channel slope, width, and sediment in actively eroding bedrock river systems. *Journal of Geophysical Research: Earth Surface*, *123*(7), 1504–1527. https://doi.org/10.1029/2017JF004405

Yanites, B. J., Tucker, G. E., Mueller, K. J., Chen, Y. G., Wilcox, T., Huang, S. Y., & Shi, K. W. (2010). Incision and channel morphology across active structures along the Peikang River, central Taiwan: Implications for the importance of channel width. *GSA Bulletin*, *122*(7–8), 1192–1208. https://doi.org/10.1130/B30035.1